



Article

Design, Modeling, and Implementation of Dual Notched UWB Bandpass Filter Employing Rectangular Stubs and Embedded L-Shaped Structure

Abdul Basit ^{1,2}, Amil Daraz ^{1,2}, Muhammad Irshad Khan ³, Najmus Saqib ⁴ and Guoqiang Zhang ^{1,*}

¹ School of Information Science and Engineering, NingboTech University, Ningbo 315104, China

² College of Information Science and Electronic Engineering, Zhejiang University, Hangzhou 310027, China

³ College of Electronics and Information Engineering, Nanjing University of Aeronautics and Astronautics (NUAA), Nanjing 210000, China

⁴ Department of Electrical Engineering, University of Engineering and Technology, Peshawar 25000, Pakistan

* Correspondence: guoqiang_zhang@nbt.edu.cn

Abstract: Targeting the range defined by the FCC (Federal Communication Commission) in 2002 for ultra-passband bandpass filters, i.e., 3.1 to 10.6 GHz, this article presents a simple compact multipoles ultra-wideband bandpass filter (range starting from 2.9 GHz and end at 11.5 GHz with central frequency 7.2 GHz) using parallel coupled microstrip line and multimode resonator with controllable double narrow notched bands at 3.5 GHz and 7.5 GHz by embedded a spur line structure and rectangular stub resonator coupled to the middle section of the multimode resonator to eliminate the interference with the existing radio signals falls in the range of 3.1 to 10.6 GHz, respectively. After optimization of the proposed filter, some attractive features were obtained, i.e., a compact size 21 mm × 5.2 mm, simple topology, good reflection coefficient lower than −18 dB, good passband transmission coefficient −1.1 dB over the entire fractional bandwidth of about 119.4%, and four transmission poles at 3.4 GHz, 4.6 GHz, 6.5 GHz, and 10 GHz, respectively, can be seen which improves the performance of the filter. Finally, the fabricated filter was tested, and the results obtained demonstrated an excellent agreement.

Keywords: bandpass filter; wireless communication; double notched bands; rectangular stub resonator; size compactness; federal communication commission



Citation: Basit, A.; Daraz, A.; Khan, M.I.; Saqib, N.; Zhang, G. Design, Modeling, and Implementation of Dual Notched UWB Bandpass Filter Employing Rectangular Stubs and Embedded L-Shaped Structure.

Fractal Fract. **2023**, *7*, 112. <https://doi.org/10.3390/fractalfract7020112>

Academic Editor: Peter Z. Petkov

Received: 18 December 2022

Revised: 19 January 2023

Accepted: 20 January 2023

Published: 23 January 2023



Copyright: © 2023 by the authors. Licensee MDPI, Basel, Switzerland. This article is an open access article distributed under the terms and conditions of the Creative Commons Attribution (CC BY) license (<https://creativecommons.org/licenses/by/4.0/>).

1. Introduction

A regulated unlicensed spectrum (3.1 GHz to 10.6 GHz) belongs to a family IEEE (Institute of Electrical and Electronics Engineers) 802.15.4 a/z called UWB (ultra-wideband) defined by FCC in 2002 with an absolute bandwidth (>500 MHz) as shown in Figure 1, was specifically designed to identify a secure and accurate real-time location of the objects. The vision behind the development of the UWB radio spectrum was “to make every connected object location aware”. The UWB spectrum is widely used in smartphones, locating essential supplies in hospitals, solving problems in industries, and applications such as smart home devices control and keyless car entry. It is 100 times more accurate than Wi-Fi or Bluetooth for locating small objects within centimeters instead of meters and mostly used in tracking objects behind walls. Furthermore, it has very low latency, unlike GPS (Global Position System), for the real-time location of fast-moving objects such as drones with a faster updating speed of up to 1000 times per second—that is 3000 times faster than Bluetooth low energy (BLE). The most important application of the UWB spectrum is to calculate the distance between the two objects, and the phenomena used for this measurement is the ToF (time of flight) which is more precise than the RSSI (received signal strength indicator) method used in Wi-Fi or BLE, respectively [1,2].

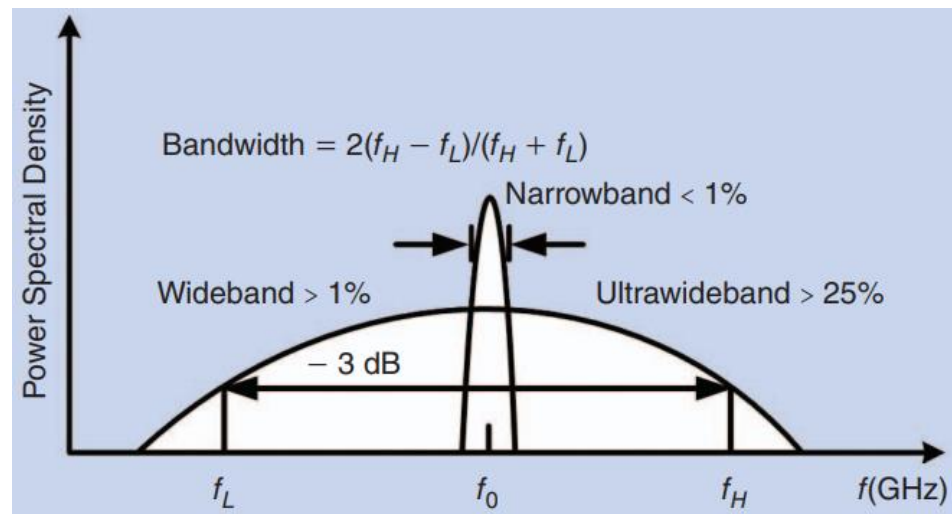


Figure 1. f_L, f_0, f_H frequencies of UWB spectrum [1].

The FCC limits the UWB power to -41.3 dBm to avoid interference with other wireless communication technologies shown in Figure 2 [3,4].

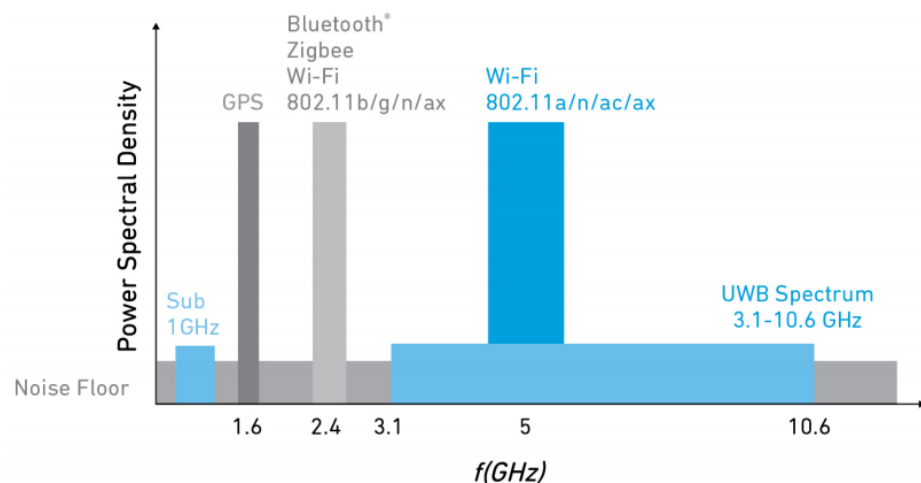


Figure 2. UWB interference with other wireless communication bands [1].

In short, the design of a bandpass filter with an ultra-passband characteristic is a difficult job for microwave researchers compared to other types of BPFs (bandpass filters). For this, continued research has been performed in the design of UWB BPFs using several techniques, such as a complementary split-ring resonator structure [5], a cascaded low and high pass filter topology [6], an interdigital parallel coupled lines [7], a coupled meandered line [8], a composite right/left-handed resonator [9], DGT (defected ground technology) [10], a multimode resonator structure [11,12], a hybrid microstrip, and a coplanar waveguide [13], etc. Recently, a UWB filter was implemented in [14] using tapered transmission line resonators for achieving the fractional bandwidth of 112.2% with wider controllable bandwidth. Initially, the main focus was on the design of a UWB filter with a good fractional bandwidth and out-of-band performance; upto 120% fractional bandwidth was achieved by the authors of [15]. Various types of notched bands at different frequencies were also achieved by the authors using different shaped resonators incorporated into the basic UWB filter design. For example, a single notch has been obtained by utilizing exponentially tapered impedance lines [15], two pairs of tightly coupled $\lambda/2$ high-impedance line resonators [16], an asymmetric trisection stepped impedance resonator [17], and an inverted T-shaped resonator in [18]. In [19,20], the authors designed a single-notched UWB

filter using quadratic Koch-island and suspended stripline structures. A $\lambda/2$ resonator loaded with three short-circuit SIS (step impedance stubs) for the implementation of single notched UWB filter at 5.1 GHz was presented in [21], but the drawback associated with the design is high insertion loss over the entire passband. Recently the authors of [22] used a complex structure for the UWB filter, but the circuit covered a larger area, although the analysis used by the authors is very good for the design of the filter. In [23–25], a microstrip to coplanar waveguide transition method was developed for the stopband creation by loading folded split ring resonators to miniaturize the circuit size and spiral resonators on the sectoral defected ground structure, but still, all these have covered a larger circuit area as compared to the structure presented in this work.

This article explores; (1) the parallel coupled microstrip line and multimode resonator structure to design an ultra-passband BPF with a circuit size $0.65 \lambda_g \times 0.16 \lambda_g$ (where λ_g is the wavelength corresponding to the central frequency of the UWB filter at 7.2 GHz); (2) a minimal modification to the geometry of the multimode resonator with a coupled rectangular stubs resonator to produce first notch band at 3.5 GHz; and (3) integration of the spur line described by the ABCD parameter analysis to the geometry of the proposed UWB filter to produce another stop band at 7.5 GHz for eliminating the WIMAX and C-band satellite downlink radio signals, respectively. The circuit size for the notched band UWB filter is $0.32 \lambda_g \times 0.08 \lambda_g$ (where λ_g is the wavelength corresponding to the central rejection frequency of 3.5 GHz). Moreover, the proposed work is fabricated and tested afterward, and the key attributes have been extracted from the fabricated design which is closely matched with the simulation results. The simulation is performed in a 3D electromagnetic (EM) simulation software Ansys HFSS version-13, while choosing a low-loss PCB [26].

This research work is organized in the following patterns: Sections 2 and 3 describe the complete analysis of the multimode resonator, spur line structure, and step impedance resonator. Section 4 shows the proposed topology, Section 5 explains how the stopbands are generated, how they will control, and how current distributed over the surface of the filter and finally, Section 6 is the conclusion of this work.

2. Ultra-Wideband Microstrip BPF Design

Calculation and Analysis of the Multimode Resonator Transmission Line

A multimode resonator microstrip line which is also called a step impedance resonator is illustrated in Figure 3a with an equivalent model in Figure 3b, which comprises two identical quarter wavelength high impedance sections with narrow strip width and one central wide strip width half wavelength low impedance transmission line that is energized with two external 50-ohm parallel coupled microstrip lines for the formation of the UWB range. The parameter Z_1, θ_1 represents the characteristics impedance and electrical length of the low impedance section, while the parameter Z_2, θ_2 represents the characteristics impedance and the electrical length of the high impedance section, respectively.

The physical structure of this resonator is identical to the structure discussed in [27]. In the later sections, it will discuss that the proposed structure has the advantage, as it utilizes all the resonance modes for the generation of the passband, whereas in [28], the first resonance mode is utilized for the actual filter design while the other modes generate the spurious harmonics. The input admittance Y_{in} of the proposed multimode resonator can be calculated using the transmission line theory equation

$$Y_{in} = jY_2 \frac{2(\tan \theta_1 + \tan \theta_2)(R - \tan \theta_1 \tan \theta_2)}{R(1 - \tan^2 \theta_1)(1 - \tan^2 \theta_2) - 2(1 + R^2) \tan \theta_1 \tan \theta_2} \quad (1)$$

where $R = Z_2/Z_1$ shows the impedance ratio of the proposed resonator, which is responsible for the adjustment of the fundamental resonant modes f_1, f_2 , and f_3 , respectively. Using the condition $Y_{in} = 0$ for resonance, the fundamental resonant modes can be extracted from the electrical lengths of both sections (θ_1 and θ_2) with the condition $\theta_2 = 2\theta_1 = \theta$ and

is calculated using Equations (2)–(6). The following equations are used to determine the physical length and the strip width of the step impedance resonator [29].

$$\theta(f_x) = \tan^{-1} \sqrt{\frac{R}{R+2}} \quad (2)$$

$$\theta(f_y) = \tan^{-1} \sqrt{\frac{R+2}{R}} \quad (3)$$

$$\theta(f_y) = \frac{\pi}{2} \quad (4)$$

$$\frac{f_y}{f_x} = \frac{\theta(f_y)}{\theta(f_x)} = \frac{\tan^{-1} \sqrt{\frac{R+2}{R}}}{\tan^{-1} \sqrt{\frac{R}{R+2}}} \quad (5)$$

$$\frac{f_z}{f_x} = \frac{\theta(f_z)}{\theta(f_x)} = \frac{\pi}{2 \tan^{-1} \sqrt{\frac{R}{R+2}}} \quad (6)$$

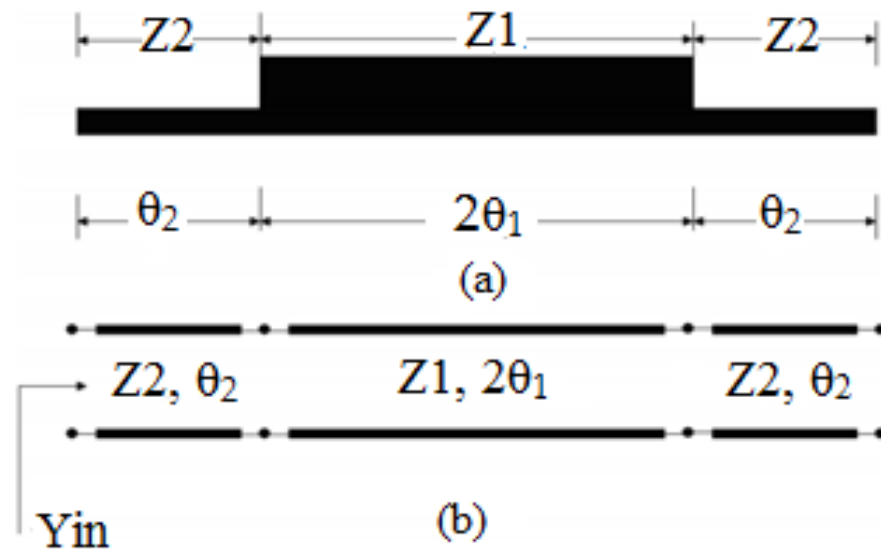


Figure 3. (a) Multimode resonator with step impedance configuration. (b) Equivalent configuration of the multimode resonator.

3. Dual Stopband Characteristic Analysis

Calculation and Analysis of the Spur Line

A spur line with its equivalent network is shown in Figure 4a,b, which consists of a pair of coupled lines, but connected at one end, and has been studied by the ABCD transmission line method. As shown in Figure 4b, the spur line has two subnetworks; N_1 , which corresponds to the microstrip line with $L = L_{s1}$, $W = W_{s1}$, and N_2 , which corresponds to the transmission line with $L = L_{s2}$, $W = W_{s2}$, where L and W represent the physical length and width of the microstrip lines with impedances Z_3 and Z_4 , respectively. The termination conditions of the spur line are as follows:

$$\begin{aligned} I_o &= I_1' + I_2' \\ V_o &= V_1' = V_2' \\ V_i &= V_1 \\ I_i &= -I_i \\ V_2 &= 0, I_2 = 0 \end{aligned} \quad (7)$$

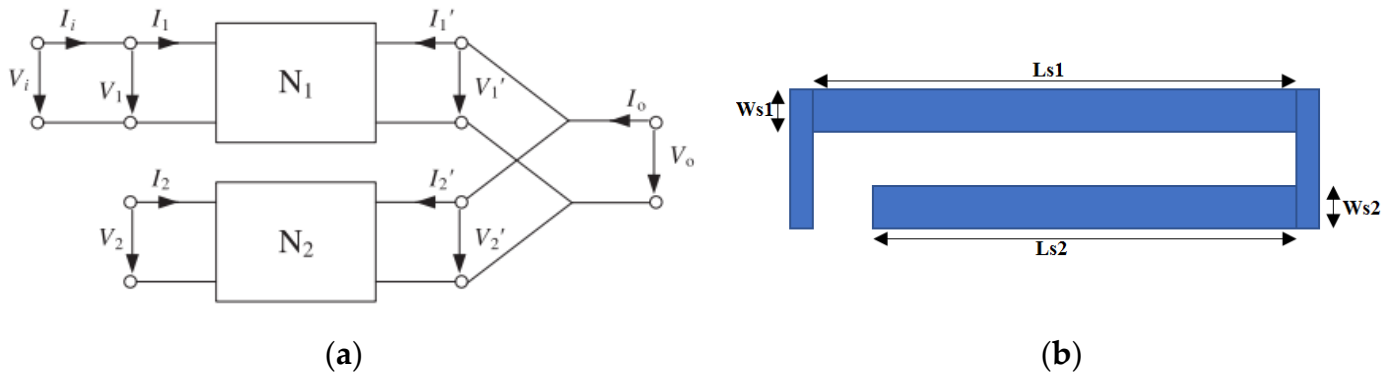


Figure 4. (a) Proposed spur line configuration. (b) Equivalent configuration of the spur line.

After the termination condition is applied to Equation (5) in [30], the four-port network becomes a two-port network. Therefore, the chain matrix is also called the ABCD matrix for the equivalent structure, having characteristic impedances Z_3 and Z_4 are

$$N_1 = \begin{pmatrix} \cos \theta_1 & jZ_3 \sin \theta_1 \\ \frac{j \sin \theta_1}{Z_3} & \cos \theta_1 \end{pmatrix} \quad (8)$$

$$N_2 = \begin{pmatrix} 1 & 0 \\ \frac{j \tan \theta_2}{Z_4 \cos \theta_2} & 1 \end{pmatrix} \quad (9)$$

Hence the final chain matrix (ABCD matrix) can be obtained by cascading Equations (8) and (9), respectively.

$$\begin{bmatrix} V_i \\ I_i \end{bmatrix} = \begin{pmatrix} Z_4 \cos \theta_2 \cos \theta_1 - Z_3 \sin \theta_1 \tan \theta_2 & jZ_3 \sin \theta_1 \\ j \frac{Z_4 \cos \theta_2 \sin \theta_1 + Z_3 \cos \theta_1 \tan \theta_2}{Z_3 Z_4 \cos \theta_2} & \cos \theta_1 \end{pmatrix} \begin{bmatrix} V_o \\ -I_o \end{bmatrix} \quad (10)$$

In terms of the ABCD matrix, it can also be written as

$$\begin{bmatrix} V_i \\ I_i \end{bmatrix} = \begin{pmatrix} A & B \\ C & D \end{pmatrix} \begin{bmatrix} V_o \\ -I_o \end{bmatrix} \quad (11)$$

where the values of A, B, C, and D are;

$$\begin{aligned} A &= \frac{Z_4 \cos \theta_1 \cos \theta_2 - Z_3 \sin \theta_1 \tan \theta_2}{Z_4 \cos \theta_2} \\ B &= jZ_3 \sin \theta_1 \\ C &= j \frac{Z_4 \sin \theta_1 \cos \theta_2 + Z_3 \cos \theta_1 \tan \theta_2}{Z_3 Z_4 \cos \theta_2} \\ D &= \cos \theta_1 \end{aligned} \quad (12)$$

In the above equations, θ shows the electrical length and is equal to βL (the propagation constant with the physical length L). The transmission coefficient S_{21} to create the stopband at a specific frequency can be calculated using the equation below [30];

$$S_{21} = \frac{2}{A + B/Z_o + CZ_o + D} \quad (13)$$

The spur line creates a notched band at a specific frequency ($S_{21} = 0$ and $Z_o = 50 \Omega$) similar to the defective ground structure in [30], which yields the following equation,

$$\cos \theta_2 = 0 \quad (14)$$

In [31,32], both the L-shaped spur line and the defective ground structure have the same slow wave features so, the fundamental frequency can be obtained from the method of the defective ground structure and is given below;

$$f_o = \frac{3 \times 10^8 \text{ m/s}}{4L_{s2}\sqrt{\epsilon_r}} \quad (15)$$

The above analysis verifies that the defective microstrip structure (DMS) is suitable for the generation of the stopband in high-frequency applications and mainly depends on the length L_{s2} having width W_{s2} of the transmission line as shown in Equation (14), i.e., by increasing the resonance frequency, the length L_{s2} will decrease. The parametric study of L_{s2} can be seen in the result and discussion section. Therefore, the analysis of the spur line discussed in this section is used for the generation of the second notch at 7.5 GHz to suppress the C-band satellite downlink in the UWB range.

Calculation and Analysis of the Rectangular Stub Resonator

The rectangular stub resonator is responsible for the creation of the first notch band at 3.5 GHz for eliminating the WiMAX wireless application and is also called a three-step impedance resonator or low–high–low impedance section, as shown in Figure 5. The length and width of the high and low impedance lines are denoted by L_a ($2\theta_a$) with W_a ($Z_5 =$ characteristic impedance of high section) and L_b (θ_b) with W_b ($Z_6 =$ characteristic impedance of low section), respectively. The impedance ratio (R) of the half wavelength step impedance resonator, when ignoring the discontinuity, is equal to the ratio of the low to high impedance sections as given below [33];

$$R = Z_6/Z_5 = \tan\theta_a \tan\theta_b \quad (16)$$

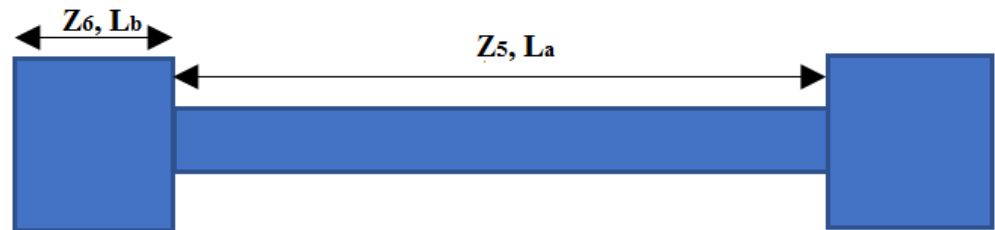


Figure 5. Proposed rectangular stub configuration.

To extend the distance between the first spurious frequency (f_{s1}) and the fundamental resonance frequency (f_o), the R should be kept as small as possible and make $\theta_a = \theta_b = \theta_o$ to achieve the resonance condition. Therefore, the mathematical equations of both the resonance condition (θ_o) and the first spurious frequency (f_{s1}) can be expressed as [34];

$$\theta_o = \tan^{-1} \sqrt{R} \quad (17)$$

$$f_{s1} = \frac{\pi f_o}{\tan^{-1} \sqrt{R}} \quad (18)$$

4. Proposed Dual-Notch UWB Topology

In this study, two filters have been designed and fabricated (1) a UWB filter having size $0.65 \lambda_g \times 0.16 \lambda_g$, and (2) a UWB filter with dual notched bands having size $0.32 \lambda_g \times 0.08 \lambda_g$ have been simulated using a 3D electromagnetic (EM) simulation software Ansys HFSS version-13 and fabricated on Rogers RO-5880 substrate with thickness 0.508 mm, dielectric loss tangent 0.0009, and relative permittivity 2.2, respectively. The device used for measuring the S-parameters was a ZNB-20 vector network analyzer, while the machine used for milling was an LPKF S63 ProtoLaser. The stopband characteristics

have been achieved using a rectangular stubs resonator to create the first notch band at 3.5 GHz and spur line structure to get the second stopband at 7.5 GHz for eliminating the WIMAX and C-band satellite downlink radio signals. The proposed topology is shown in Figure 6, along with dimensions in millimeters (mm) listed in Table 1.

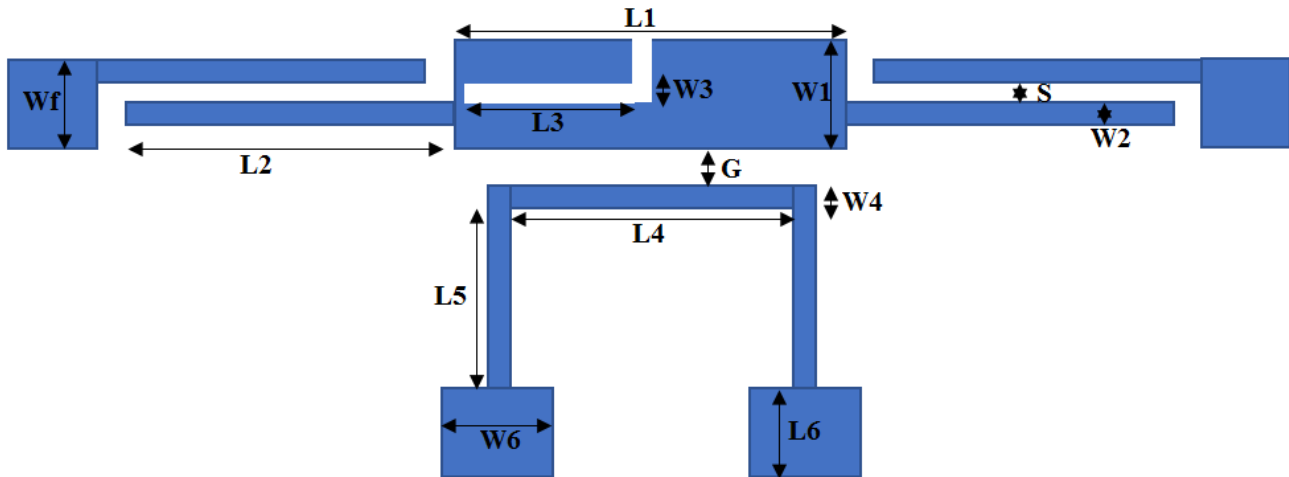


Figure 6. Schematic diagram of the dual-notched UWB BPF.

Table 1. Proposed filter dimensions in mm.

L	21	W	5.2	L ₁	7.52	W ₁	1.08
L ₂	4.13	W ₂	0.1	L ₃	4.15	W ₃	0.1
L ₄	5	W ₄	0.25	L ₅	0.75	L ₆	2.8
W ₆	1.8	W _f	1.48	S	0.05	G	0.3

5. Experimental Result Discussion of the Proposed UWB BPF with Notched Bands

As discussed above, the three resonance modes ($f_1 = 3.9$ GHz, $f_2 = 7$ GHz, and $f_3 = 9.6$ GHz) appeared due to the frequency distributed coupling of the parallel coupled microstrip line of the multimode resonator with space $S = 0.05$ mm is responsible for the building of the novel multipole UWB BPF design. Figure 7 shows the magnitude of the simulated and measured S_{11} and S_{21} plots of the UWB BPF. Under weak coupling ($L_2 = 0.5$ mm) of the parallel coupled microstrip line, only two transmission poles could be observed, but when the coupling gets stronger and stronger by enlarging the length L_2 , the number of transmission poles also increased within the passband of the UWB BPF, as shown in Figure 8. Now looking at Figures 8 and 9, when the length L_2 was enlarged from 0.5 to 1.5 mm, the return loss fell gradually, while the insertion loss rose up and further increased the length L_2 to 3.9 mm, which was approximately equal to the $\lambda/4$, the S_{21} shifted to make an ultrawideband BPF with one additional pole and, thus, a total of four transmission poles appeared in the S_{11} at different frequencies, as shown in Figure 9. In this way, a planar compact ultra-passband filter with an effective circuit area of $0.65 \lambda_g \times 0.16 \lambda_g$, fractional bandwidth of 119.4%, insertion loss of -1.1 dB, and $S_{11} > 18$ dB is implemented in HFSS and fabricated on the low-cost substrate material, respectively.

Now, the attention is shifted to how notched bands are formed in the ultrawide passband filter. As discussed above, the two stopbands are formed by the embedded spur line and rectangular stub resonator coupled to the middle section of the proposed multimode resonator structure with the gap $G = 0.3$ mm. The first notch band for eliminating the frequency at 3.5 GHz was obtained due to the rectangular stubs coupled to the main transmission line, while the second notch band obtained for eliminating the frequency at 7.5 GHz was due to the L-shaped spur line structure, as shown in the Figures 10 and 11, respectively. The first stopband was obtained when the gap between the rectangular stub

resonator and the multimode resonator was kept small. Thus, the first stopband appeared when the rectangular stub resonator was strongly coupled to the multimode resonator with a gap $G = 0.3$ mm. As shown in Figure 10, when the gap increased from 0.3 mm to 0.5 mm, the first stopband peak vanished and went towards -10 dB.

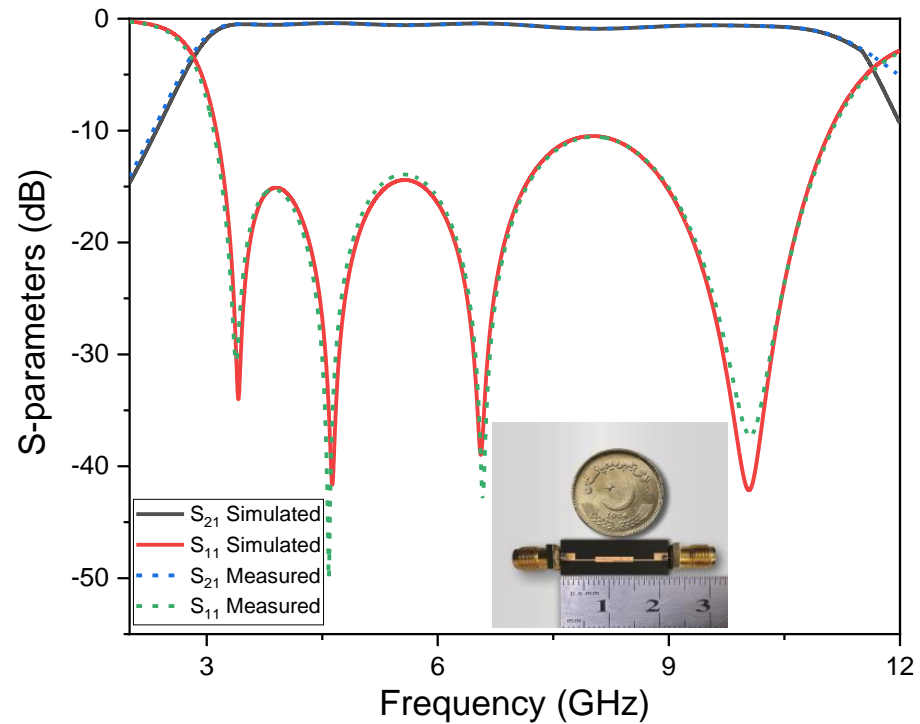


Figure 7. Simulated and measured S_{11} and S_{21} frequency plots of the initial UWB BPF.

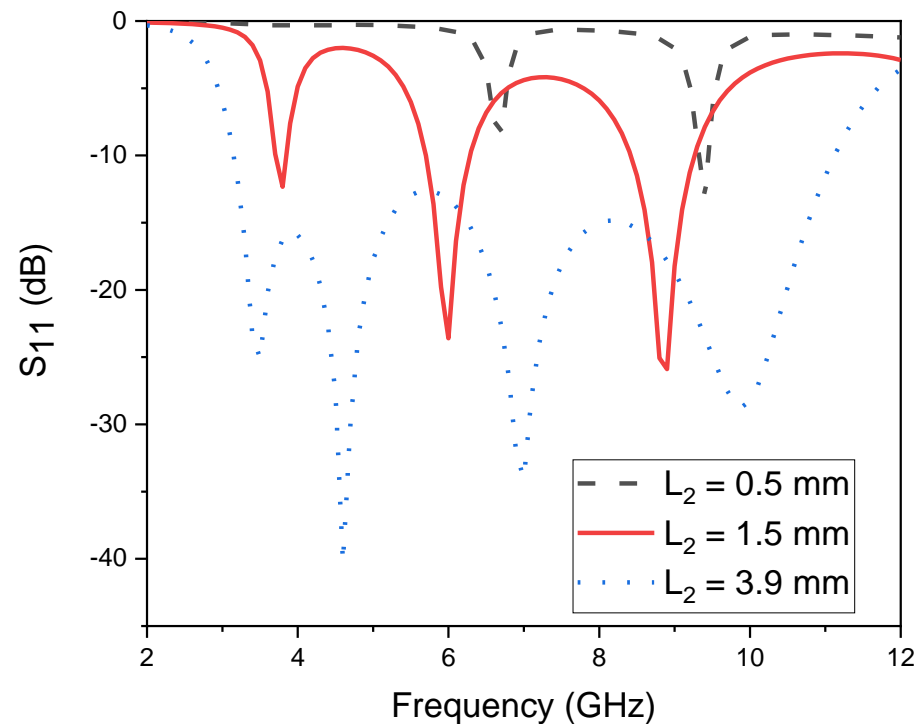


Figure 8. Transmission poles appearance w.r.t parameter L_2 .

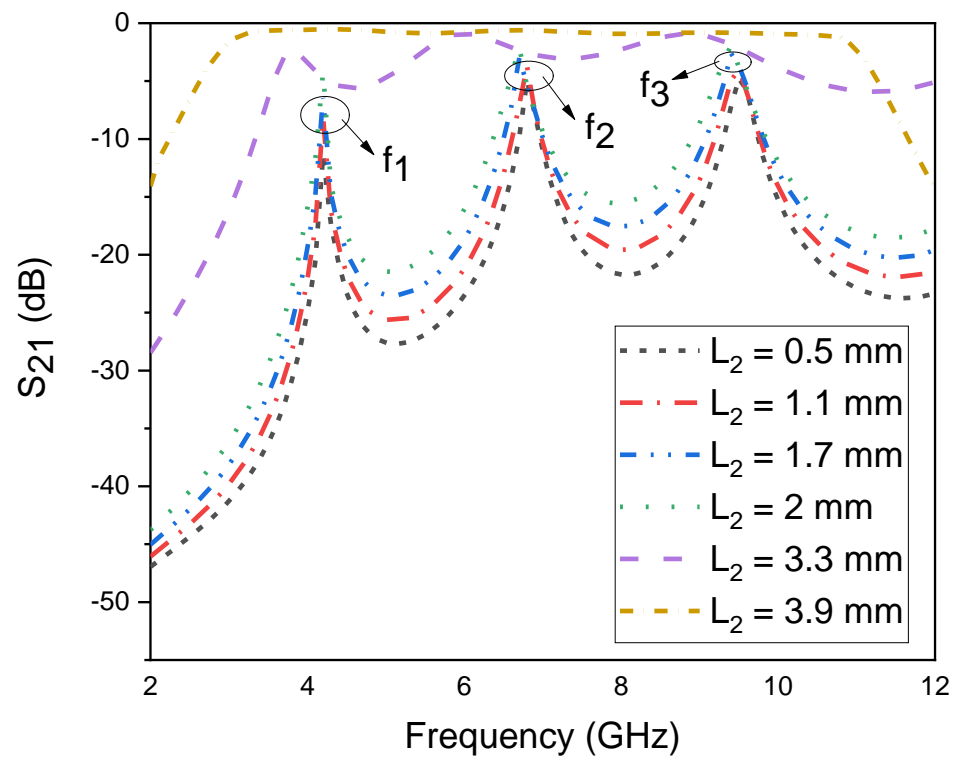


Figure 9. The magnitude of $|S_{21}|$ under different coupling scheme w.r.t parameter L_2 .

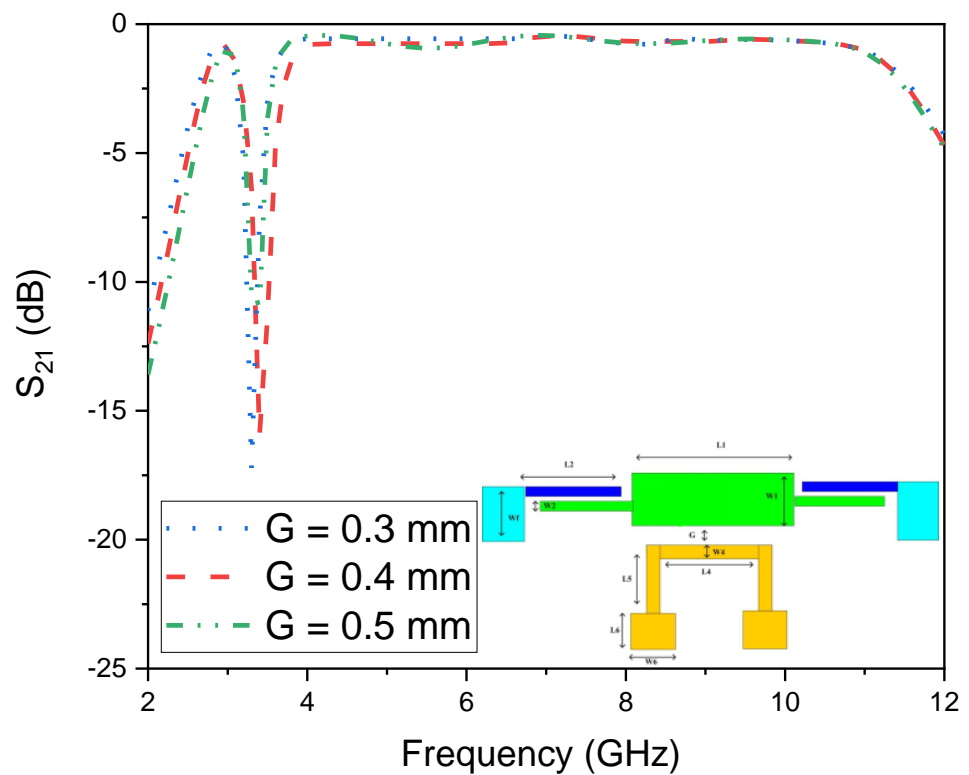


Figure 10. S_{21} plot of UWB notch filter with proposed rectangular stubs.

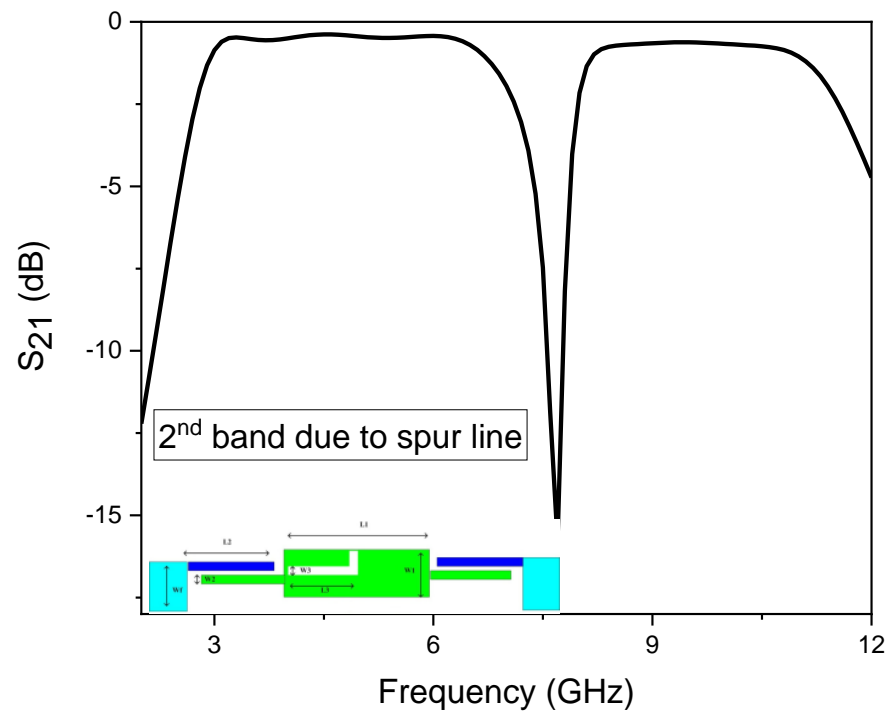


Figure 11. S_{21} plot of UWB notch filter with embedded spur line structure.

The interesting property of the proposed filter is the independently controlled of both stopbands with the parameters L_4 , L_5 , W_6 , L_3 , and W_3 , i.e., by enlarging the parameter L_4 from 2 mm to 5 mm, a large variation could be seen in the first stopband, while the second notch band was almost constant, as shown in Figure 12. Similarly, by varying the width W_6 and the length L_5 , a small variation was again obtained, while the second notch band at 7.5 GHz was not changed, as illustrated in Figures 13 and 14, respectively.

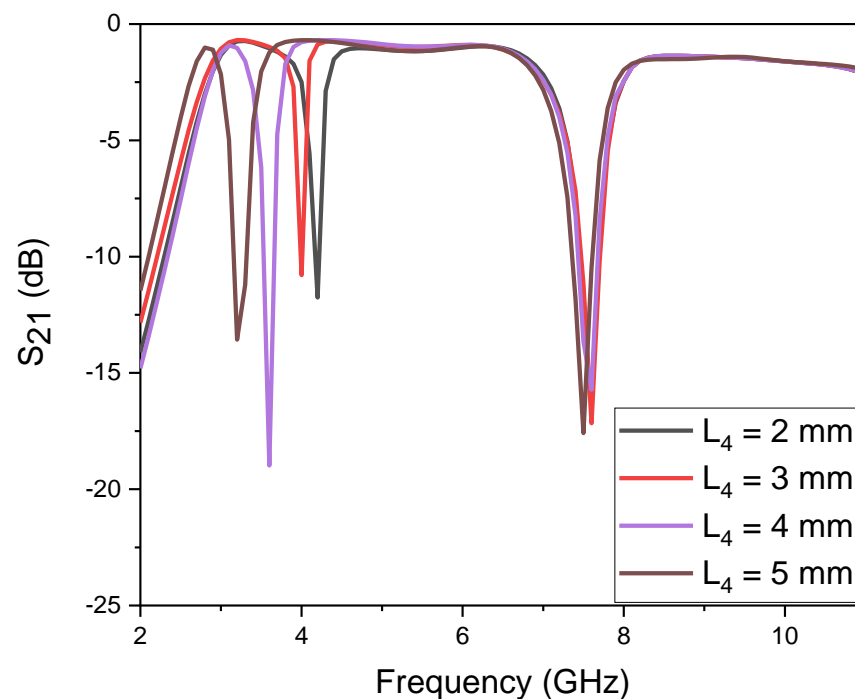


Figure 12. S_{21} plot of first band control with parameter L_4 .

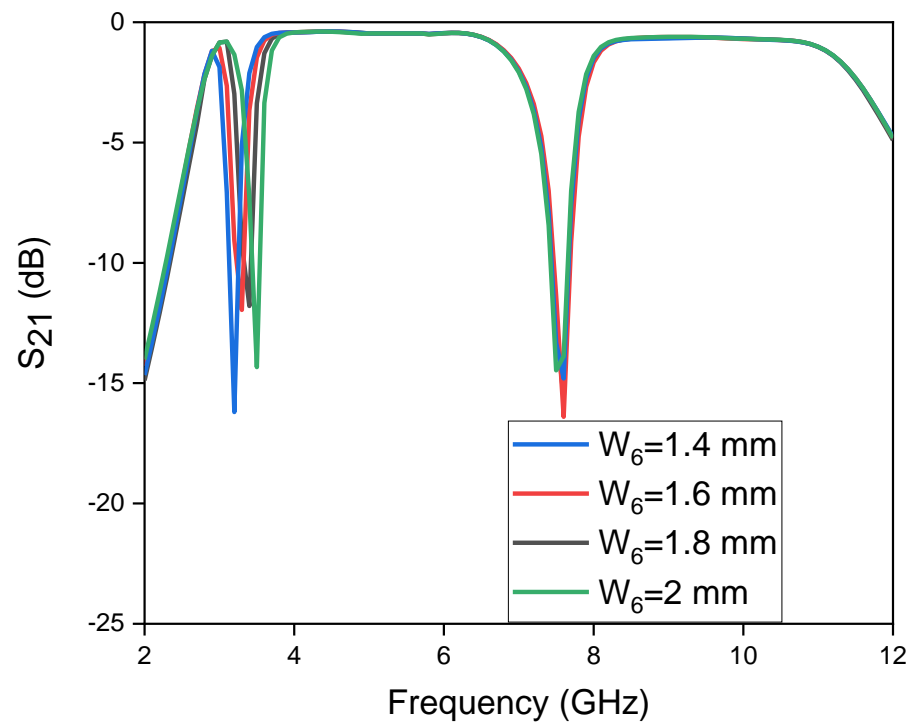


Figure 13. S_{21} plot of first band control with parameter W_6 .

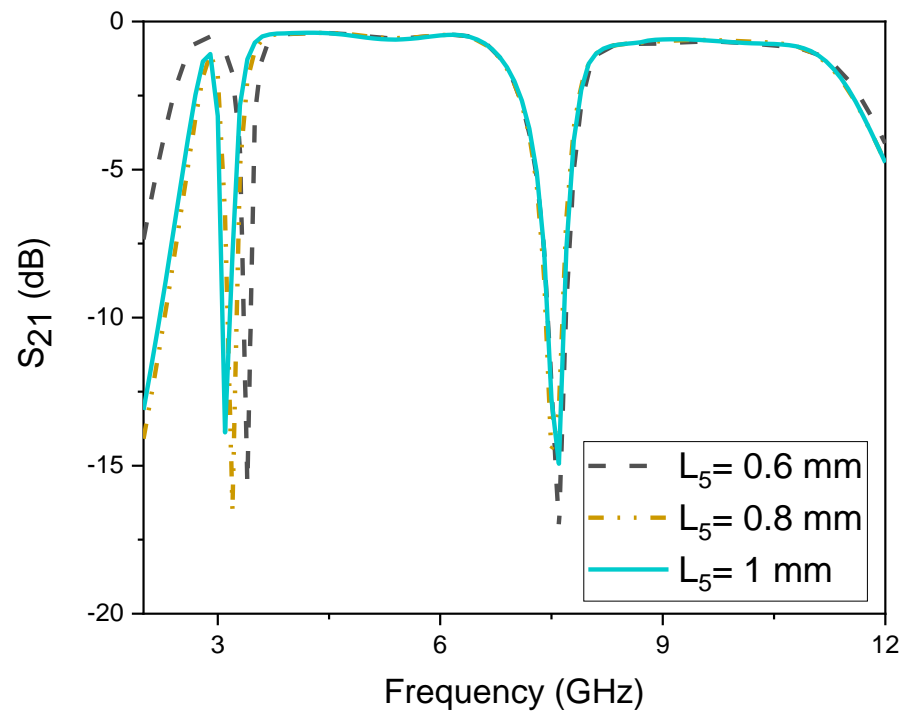


Figure 14. S_{21} plot of first band control with parameter L_5 .

The second notch band at 7.5 GHz is mainly controlled with the parameters L_3 and W_3 , i.e., by small changes in the length L_3 from 3.8 mm to 4.1 mm, a large variation can be seen, as shown in Figure 15, while the first stopband was constant. Similarly, when the width W_3 increased from 0.1 mm to 0.4 mm, a reasonable change occurred in the second band, while keeping the first stopband constant, as given in Figure 16.

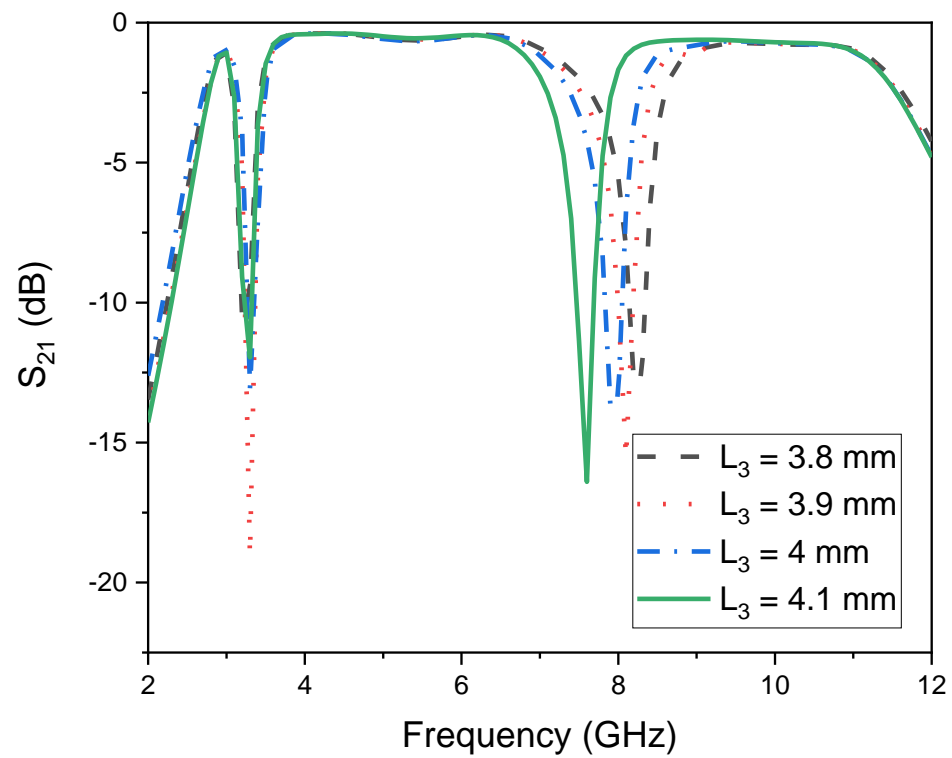


Figure 15. S_{21} plot of second band control with parameter L_3 .

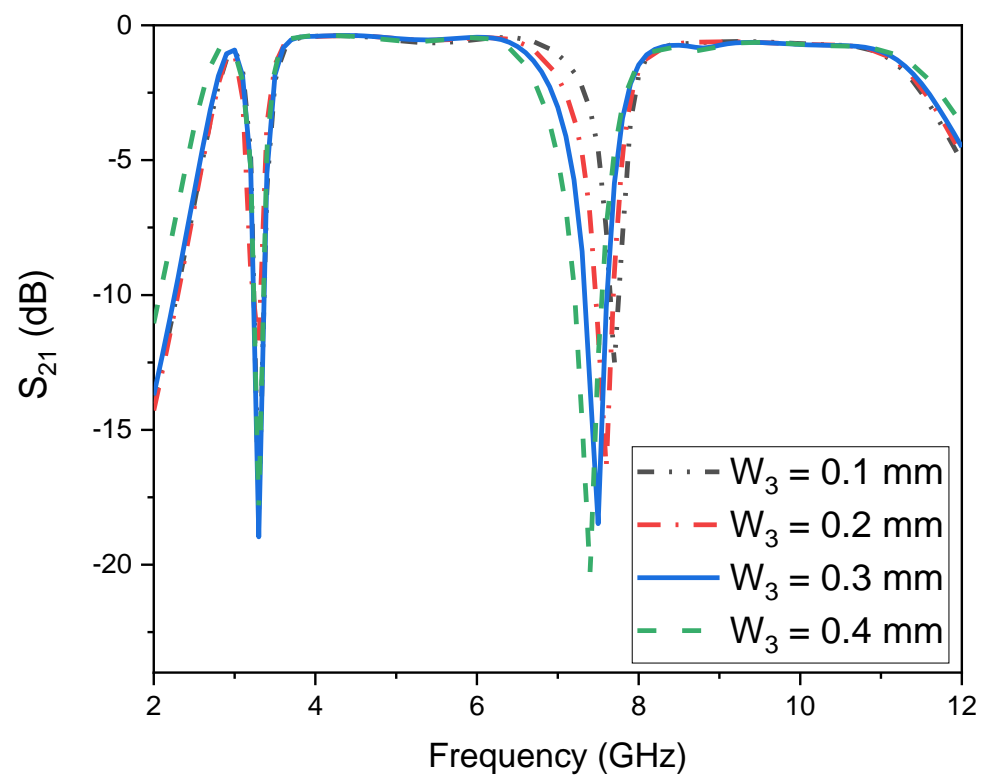


Figure 16. S_{21} plot of second band control with parameter W_3 .

The next important concept that needs to be discussed is the current distribution. It is used to confirm the resonant conditions of the proposed filters. Figure 17 shows the simulated current distributions at the center frequency of the passband response, from 2.8 to 11.5 GHz. As discussed, the strong coupling effect of the parallel coupled lines L_2

with narrow space (S) was utilized to excite the ultra-wideband response, as shown in Figures 8 and 9. Therefore, most current energy is absorbed by these lines, thus creating a UWB response. Figure 18 shows the simulated current distributions of the notched filter at a frequency of 3.5 GHz. As discussed above, when the rectangular resonator is coupled with gap G to the multimode resonator, as shown in Figure 10, the first stop band at 3.5 GHz is created. The coupled stub absorbs a relatively high amount of current energy, and this is further verified in Figure 12 by varying the stub L_4 . Similarly, when the spur line is embedded in the multimode resonator, as shown in Figure 11, the second stopband is achieved at a frequency of 7.5 GHz. The simulated current distributions of the notched filter are observed at this specific frequency near the spur line, as shown in Figure 19. The final graphical record of the current distribution for both notches is shown in Figure 20.

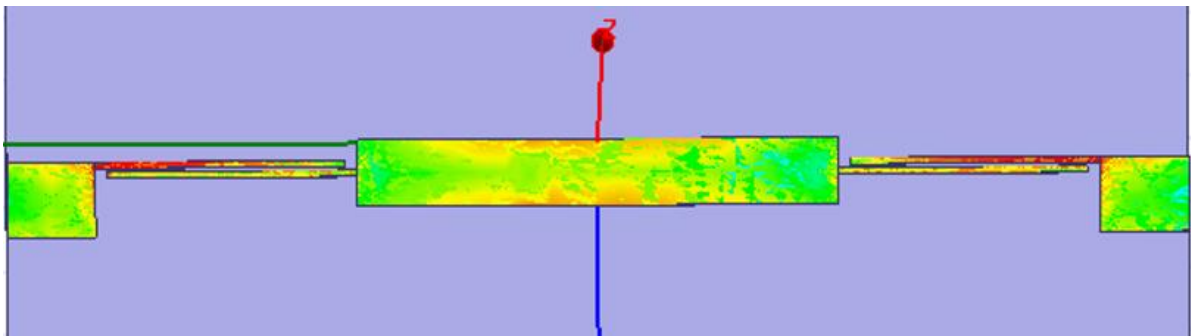


Figure 17. Current distribution of the UWB filter at central frequency 7.2 GHz.

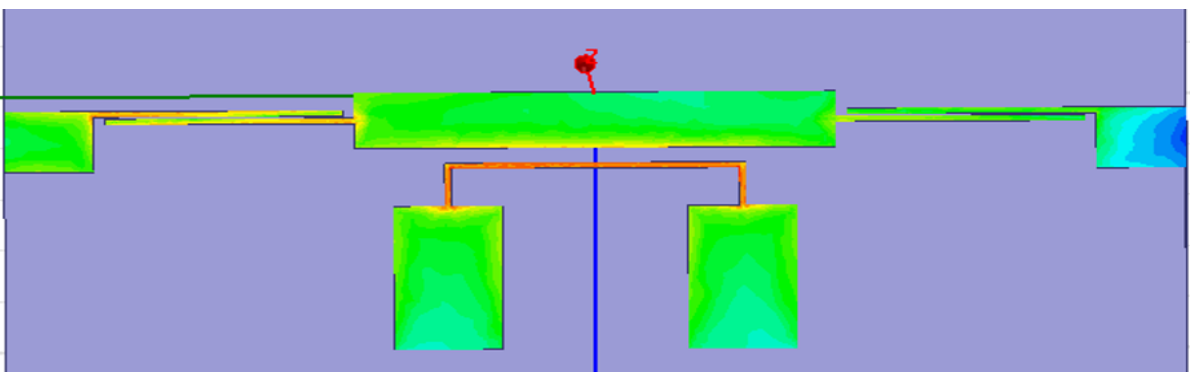


Figure 18. Current distribution of the UWB filter with a notch at 3.5 GHz.

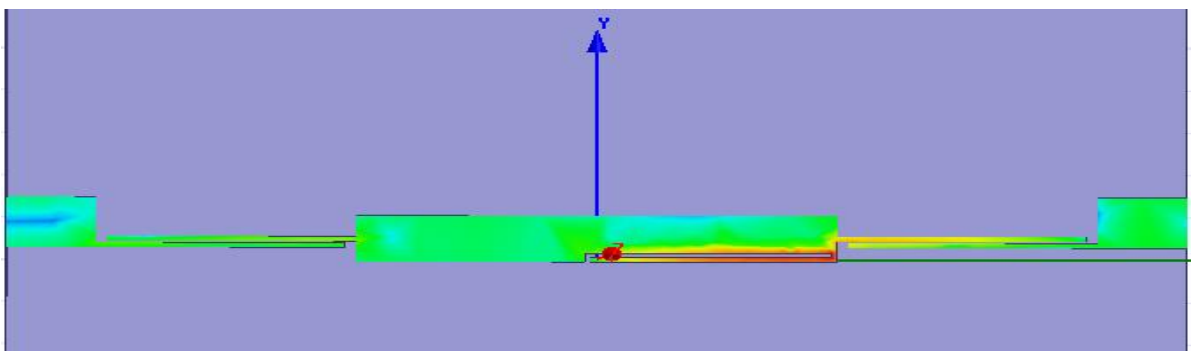


Figure 19. Current distribution of the UWB filter with a notch at 7.5 GHz.

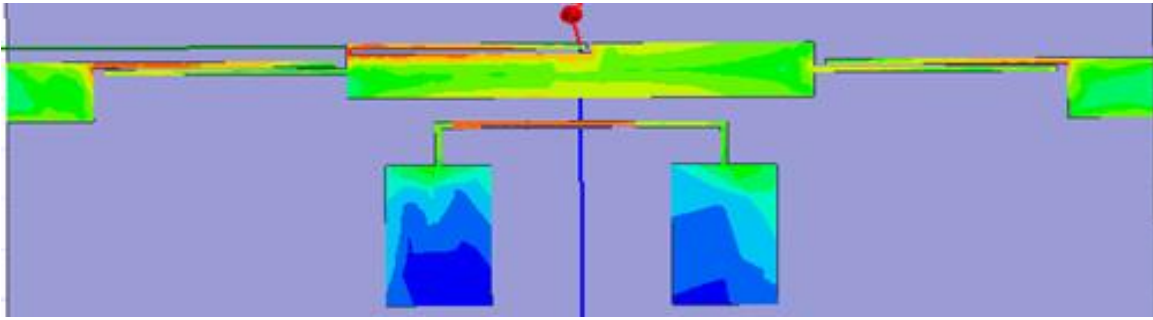


Figure 20. Current distribution of the UWB filter with dual notched band characteristics.

This verifies that the proposed structure eliminates the potential interference in ultra-wideband microwave applications and has the advantage of stopping unwanted wireless bands according to the user's need. In this research work, the novelty is claimed by using a simple topology to reduce the cost and then compared with the most recent articles published in reputed journals/conferences in terms of its small circuit size, good FBW, low insertion loss over the entire UWB range, high returns loss, and independently controlled notch bands which are tabulated in Table 2, respectively. Moreover, the final S_{11} and S_{21} frequency plots of the proposed dual notch UWB BPF, with a fabricated photograph, are shown in Figure 21.

Table 2. Comparison with other reported work.

Ref.	Passband (GHz)	FBW (%)	S_{11} , S_{21} (dB)	No. of Notches	Circuit Size ($\lambda_g \times \lambda_g$)
[16]	3.4–10	98.5	22.7, 0.7	1	1.09×0.44
[17]	2.86–10.72	115.7	>40, <1	1	0.67×0.46
[19]	3.38–9.7	96	21.2, 0.39	1	1.02×1.08
[20]	2.9–10.6	114	19, <1.3	1	0.73×0.34
[22]	2.15–11.18	129.5	>10, 1.5	1	0.80×0.42
[23]	2.75–10.7	118	15.5, <0.87–<1.8	2	1.01×0.76
[24]	2.9–10.5	113	15.5, 1	2	1.01×0.76
[25]	3–10.9	113.6	>15, 0.6	2	0.90×0.51
[35]	3.25–10.73	106	17.3, 0.8	2	1.34×0.41
Filter1	2.9–11.5	119.4	>10, <1.1	No	0.65×0.16
Filter2	2.9–11.5	119.4	>18, <1.1	2	0.32×0.08

FBW = fractional bandwidth, S_{21} = insertion loss, S_{11} = return loss $\lambda_g = 7.2$ GHz for filter 1 and 3.5 GHz for filter 2.

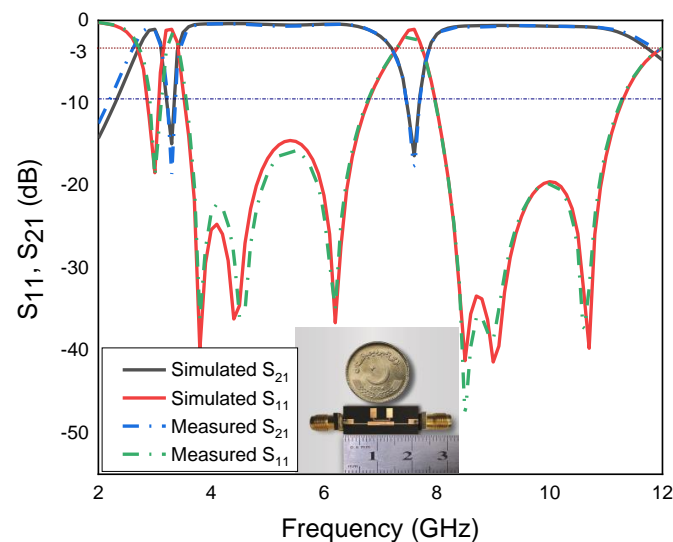


Figure 21. EM-simulated and measured frequency plots responses of the proposed dual-notched UWB-BPF.

6. Conclusions

This article presented a new compact multipoles UWB BPF with adjustable dual stop-band frequencies using extremely high coupled parallel microstrip lines with embedded spur line structure and rectangular stub resonator to suppress the unwanted frequency signals at 3.5 GHz for WiMAX with an absolute bandwidth of 310 MHz and 7.5 GHz with an absolute bandwidth 690 MHz for C-band satellite downlink communication system, respectively. The filter has some attractive features such as compact size, good reflection coefficient lower than -18 dB, good insertion loss of -1.1 dB over the entire passband, and multiple transmission poles, which made the proposed filter much better than those discussed in the literature. Finally, the filter has been measured and tested, and the results obtained were in good agreement.

Author Contributions: Conceptualization, A.B. and G.Z.; methodology, A.B.; software, A.B., N.S., M.I.K. and A.D.; formal analysis, A.D.; investigation, A.B.; resources, A.D.; data curation, A.B.; writing—original draft preparation, A.B.; writing—review and editing, G.Z.; visualization, A.B. and A.D.; supervision, G.Z.; project administration, G.Z.; funding acquisition, G.Z. All authors have read and agreed to the published version of the manuscript.

Funding: This work is supported by “Young Talent Sub-project of Ningbo Yongjiang Talent Introduction Programme under grant no 20100859001.”

Data Availability Statement: Not applicable.

Conflicts of Interest: The authors declare no conflict of interest.

References

- Wang, L.T.; Xiong, Y.; He, M.; Kheir, M. Review on UWB bandpass filters. In *UWB Technology-Circuits and Systems*; IntechOpen: London, UK, 2019; pp. 1–24.
- FCC. *Revision of Part 15 of the Commission’s Rules Regarding Ultra-Wideband Transmission System*; FCC: Washington, DC, USA, 2002.
- Khattak, M.I.; Khan, M.I.; Anab, M.; Ullah, A.; Al-Hasan, M.; Nebhen, J. Miniaturized CPW-fed UWB-MIMO antennas with decoupling stub and enhanced isolation. *Int. J. Microw. Wirel. Technol.* **2022**, *14*, 456–464. [[CrossRef](#)]
- Basit, A.; Khattak, M.I.; Zubir, F.; Shah, S.W. Miniaturized ultra-wideband filter with independently controlled notch bands for 5.1/6/8 GHz wireless applications. *PLoS ONE* **2022**, *17*, e0268886. [[CrossRef](#)] [[PubMed](#)]
- Sarkar, D.; Moyra, T.; Murmu, L. An ultra-wideband (UWB) bandpass filter with complementary split ring resonator for coupling improvement. *Int. J. Electron. Commun.* **2017**, *71*, 89–95. [[CrossRef](#)]
- Gomez-Garcia, R.; Alonso, J.I. Systematic method for the exact synthesis of ultra-wideband filtering responses using high-pass and low-pass sections. *IEEE Trans Microw Theory Tech.* **2006**, *54*, 3751–3764. [[CrossRef](#)]
- Xia, X.; Chen, F.; Cheng, X.; Deng, X. A compact ultra-wideband bandpass filter with good selectivity based on interdigital coupled-line. *Int. J. RF Microw. Comput. -Aided Eng.* **2018**, *28*, e21419. [[CrossRef](#)]
- Jiang, Y.; Tang, W.; Shi, Y.; Zhou, P.; Feng, L. Compact and low insertion loss UWB on-chip bandpass filter using coupled meandered line. *Microw. Opt. Technol. Lett.* **2020**, *62*, 2236–2242. [[CrossRef](#)]
- Li, C.; Tong, C.; Qi, L.; Zou, X.; Ji, M. Multimode resonator based on composite right-/left-handed transmission line for UWB bandpass filter application. *Int. J. RF Microw. Comput. -Aided Eng.* **2015**, *25*, 815–824. [[CrossRef](#)]
- Sahu, B.; Singh, S.; Meshram, M.K.; Singh, S.P. Super-compact ultra-wideband microstrip band-pass filter with improved performance using defected ground structure-based low-pass filter. *J. ElectromagnEtic WavEs Appl.* **2018**, *32*, 635–650. [[CrossRef](#)]
- Kumar, S.; Gupta, R.D.; Parihar, M.S. Multiple band notched filter using C-shaped and E-shaped resonator for UWB applications. *IEEE Microw. Wirel. Compon. Lett.* **2016**, *26*, 340–342. [[CrossRef](#)]
- Shome, P.P.; Khan, T. A compact design of circular-ring shaped MMR based bandpass filter for UWB applications. In Proceedings of the 2019 IEEE Asia-Pacific Microwave Conference (APMC), Singapore, 13 December 2019.
- Kuo, T.N.; Lin, S.C.; Chen, C.H. Compact ultra-wideband bandpass filter using composite microstrip-coplanar-waveguide structure. *IEEE Trans. Microw. Theory Tech.* **2006**, *54*, 3772–3778. [[CrossRef](#)]
- Razzaz, F.; Saeed, S.M.; Alkanhal, M.A. Ultra-Wideband Bandpass Filters Using Tapered Resonators. *Appl. Sci.* **2022**, *12*, 3699. [[CrossRef](#)]
- Sangam, R.S.; Kshetrimayum, R.S. Notched UWB filter using exponential tapered impedance line stub loaded microstrip resonator. *J. Eng.* **2018**, *2018*, 768–772. [[CrossRef](#)]
- Weng, M.H.; Hsu, C.W.; Lan, S.W.; Yang, R.Y. An ultra-wideband bandpass filter with a notch band and wide upper bandstop performances. *Electronics* **2019**, *8*, 1316. [[CrossRef](#)]
- Kumari, P.; Sarkar, P.; Ghatak, R. A multi-stub loaded compact UWB BPF with a broad notch band and extended stopband characteristics. *Int. J. RF Microw. Comput. Aided Eng.* **2020**, *30*, e22138. [[CrossRef](#)]

18. Ranjan, P.; Kishore, N.; Dwivedi, V.K.; Upadhyay, G.; Tripathi, V.S. UWB filter with controllable notch band and higher stop band transmission zero using open stub in inverted T-shaped resonator. In Proceedings of the 2017 IEEE Asia Pacific Microwave Conference (APMC), Kuala Lumpur, Malaysia, 13 November 2017; pp. 817–820.
19. Bhaskar, M.; Mathew, T. Ultra-wideband bandpass filter with notch band based on quadratic Koch island structure. *Indones. J. Electr. Eng. Inform.* **2021**, *9*, 793–798. [[CrossRef](#)]
20. Xu, Z. UWB bandpass SSL filter with an adjustable notched band and four transmission zeros. *Electron. Lett.* **2021**, *57*, 930–932. [[CrossRef](#)]
21. Liu, L.Q.; Lai, H.S.; Hu, H.M.; Chen, J.J.; Weng, M.H.; Yang, R.Y. A Simple Method to Design a UWB Filter with a Notched Band Using Short-Circuit Step Impedance Stubs. *Electronics* **2022**, *11*, 1124. [[CrossRef](#)]
22. Bandyopadhyay, A.; Sarkar, P.; Ghatak, R. A Bandwidth Reconfigurable Bandpass Filter for Ultrawideband and Wideband Applications. *IEEE Trans. Circuits Syst. II Express Briefs* **2022**, *69*, 2747–2751. [[CrossRef](#)]
23. Ghazali, A.N.; Sazid, M.; Pal, S. A miniaturized low-cost microstrip-to-coplanar waveguide transition-based ultra-wideband bandpass filter with multiple transmission zeros. *Microw. Opt. Technol. Lett.* **2020**, *62*, 3662–3667. [[CrossRef](#)]
24. Ghazali, A.N.; Sazid, M.; Pal, S. Multiple passband transmission zeros embedded compact UWB filter based on microstrip/CPW transition. *Int. J. Electron. Commun.* **2021**, *129*, 1–6. [[CrossRef](#)]
25. Ghazali, A.N.; Sazid, M.; Pal, S. A dual notched band UWB-BPF based on microstrip-to-short circuited CPW transition. *Int. J. Microw. Wirel. Technol.* **2018**, *10*, 794–800. [[CrossRef](#)]
26. Ansoft Corporation. Ansoft HFSS, version 13. Available online: <https://www.ansys.com/products/electronics/ansys-hfss> (accessed on 17 December 2022).
27. Hsieh, L.H.; Chang, K. Compact, low insertion-loss, sharp-rejection, and wide-band microstrip bandpass filters. *IEEE Trans. Microw. Theory Tech.* **2003**, *51*, 1241–1246. [[CrossRef](#)]
28. Makimoto, M.; Yamashita, S. Bandpass filters using parallel coupled stripline stepped impedance resonators. *IEEE Trans. Microw. Theory Tech.* **1980**, *28*, 1413–1417. [[CrossRef](#)]
29. Gupta, K.C.; Garg, R.; Bahl, I.; Bhartia, P. *Microstrip Lines and Slotlines*, 2nd ed.; Artech House: Norwood, MA, USA, 1996.
30. Bates, R.N. Design of microstrip spur-line band-stop filters. *IEEE J. Microw. Opt. Acoust.* **1977**, *1*, 209–214. [[CrossRef](#)]
31. Wang, J.; Ning, H.; Xiong, Q.; Li, M.; Mao, L.F. A novel miniaturized dual-band bandstop filter using dual-plane defected structures. *Prog. Electromagn. Res.* **2013**, *134*, 397–417. [[CrossRef](#)]
32. Hong, J.S.; Karyamapudi, B.M. A general circuit model for defected ground structures in planar transmission lines. *IEEE Microw. Wirel. Compon. Lett.* **2015**, *15*, 706–708. [[CrossRef](#)]
33. Basit, A.; Khattak, M.I.; Althuwayb, A.; Nebhen, J. Compact Tri-band Bandpass Filter Based on Asymmetric Step Impedance Resonators for WiMAX and RFID Systems. *J. Electromagn. Eng. Sci.* **2021**, *21*, 316–321. [[CrossRef](#)]
34. Basit, A.; Khattak, M.I.; Nebhen, J.; Jan, A.; Ahmad, G. Investigation of external quality factor and coupling coefficient for a novel SIR based microstrip tri-band bandpass filter. *PLoS ONE* **2021**, *16*, e0258386. [[CrossRef](#)]
35. Sazid, M.; Raghava, N.S. Planar UWB-bandpass filter with multiple passband transmission zeros. *Int. J. Electron. Commun.* **2021**, *134*, 1–7. [[CrossRef](#)]

Disclaimer/Publisher’s Note: The statements, opinions and data contained in all publications are solely those of the individual author(s) and contributor(s) and not of MDPI and/or the editor(s). MDPI and/or the editor(s) disclaim responsibility for any injury to people or property resulting from any ideas, methods, instructions or products referred to in the content.